HHS Public Access

Author manuscript

*J Refract Surg*. Author manuscript; available in PMC 2018 August 03.

Published in final edited form as:

*J Refract Surg*. 2016 December 01; 32(12): 811–820. doi:10.3928/1081597X-20160929-01.

# Computational Biomechanical Analysis of Asymmetric Ectasia Risk in Unilateral Post-LASIK Ectasia

**Ali Vahdati, PhD**, **Ibrahim Seven, PhD**, **Naveen Mysore, MD, PhD**, **J. Bradley Randleman, MD**, and **William J. Dupps Jr., MD, PhD**

Cole Eye Institute, Cleveland Clinic, Cleveland, Ohio (AV, IS, NM, WJD); the Department of Ophthalmology, Emory University, Atlanta, Georgia (JBR); and the Department of Biomedical Engineering, Cleveland Clinic, Cleveland, Ohio (WJD)

## Abstract

**Purpose—**To develop a computational approach to corneal biomechanical risk analysis in refractive surgery and to investigate its utility in an enigmatic case of unilateral ectasia after bilateral LASIK.

**Methods—**Preoperative corneal elevation datasets from both eyes of a patient who developed unilateral post-LASIK ectasia were used to construct geometrically patient-specific, microstructurally motivated finite element models. Models were assessed before and after implementation of case-specific treatment parameters for interocular differences in corneal geometry and strain behavior under physiological loading conditions.

**Results—**Standard clinical predictors of post-LASIK ectasia risk were similar for the affected and contralateral eyes, and no risk factor asymmetry was identified in tomographic screening that included posterior corneal elevation analysis. However, differences in the magnitude and distribution of strain and stress were observed that are consistent with greater predisposition to biomechanical instability in the affected eye. Load testing with simulated intraocular pressure increases provoked opposite trends in curvature change in the preoperative models representing affected and unaffected eyes, with steepening in the ectatic eye and flattening in the clinically stable eye.

**Conclusions—**Patient-specific computational analyses revealed differences in intrinsic biomechanical behaviors that may predispose a cornea to instability after refractive surgery. Strain and stress analyses elucidated differential risk not ascertained with current refractive surgery screening paradigms. This pilot study illustrates a risk analysis approach that implicitly considers the entire corneal three-dimensional geometry and can be performed a priori in a screening setting.

*Correspondence*: William J. Dupps, Jr., MD, PhD, Cole Eye Institute, 9500 Euclid Ave., i-32, Cleveland OH 44195, bjdupps@sbcglobal.net.

Dr. Seven is a consultant and Dr. Randleman is a Scientific Advisory Board Member for OptoQuest. Dr. Dupps has intellectual property in computational modeling filed with Cleveland Clinic and licensed to OptoQuest, has sponsored research for Carl Zeiss Meditec and Avedro, and is a consultant for Ziemer. The remaining authors have no financial or proprietary interest in the materials presented herein.

Dr. Randleman did not participate in the editorial review of this manuscript.

**Author Contributions**

Study concept and design (AV, JBR, WJD); data collection (JBR); analysis and interpretation of data (AV, IS, NM, JBR, WJD); writing the manuscript (AV, JBR, WJD); critical revision of the manuscript (IS, NM, JBR, WJD); supervision (WJD)

Postoperative corneal ectasia is a rare complication of keratorefractive surgery characterized by progressive localized steepening, increasing refractive error with irregular astigmatism, and potential loss of corrected distance visual acuity.[1,2] Detecting risk propensity remains one of the most challenging issues in the evaluation of potential refractive surgery candidates, in part due to the complex interaction of intrinsic (patient) and extrinsic (surgical) risk factors.[5–8]

Several studies have reported potential risk factors for occurrence of postoperative corneal ectasia, including the statistically based Ectasia Risk Score System (ERSS).[9] This screening paradigm has proven useful by supporting a semi-quantitative approach to screening that integrates multiple patient and surgical risk factors in a straightforward grading scheme; however, limitations include the need for subjective grading of a major risk driver (corneal topography) and the use of one-dimensional structural risk factors related to central corneal thickness that do not capture the three-dimensional interaction of spherical and astigmatic ablation profiles with corneal structure.[10,11] The percent tissue altered provides a thickness-specific assessment of the extrinsic factors by relating surgical invasiveness to preoperative central corneal thickness but does not address corneal curvature factors.[6,12] Many additional screening approaches have been described using patient-specific tomographic data, including posterior elevation and relational thickness analyses from Scheimpflug tomography,[13,14] but a unified, universal scheme for risk screening that includes comprehensive tomographic and procedure-specific data has yet to be developed and validated.

Advances in computational medicine offer unprecedented opportunities for assessing the structural impact of the three-dimensional interaction of planned treatments with corneal structure.[8,10] This report describes a computational method for analysis of corneal structural risk and pilots the approach in the enigmatic setting of unilateral post-LASIK ectasia. In addition to assessing the utility of this computational approach as a tool for preoperative clinical screening, we sought to generate the first structural analysis of a clinical case of ectasia using preoperative patient-specific corneal geometry data alone and in combination with simulation of case-specific LASIK procedures.

## Patients and Methods

### Clinical Case

A 30-year-old man who underwent uneventful bilateral LASIK in 2009 achieved 20/20 uncorrected distance visual acuity initially but presented with decreased acuity and tomographic evidence of unilateral ectasia in the right eye 18 months postoperatively. The LASIK procedure was performed using the Alcon WaveLight Allegretto 400-Hz excimer laser (Alcon Laboratories, Inc., Fort Worth, TX) and the Amadeus II Microkeratome (Ziemer Ophthalmic, Port, Switzerland) using ML7090 CLB blades distributed by Med-Logics, Inc. Thickness profiles of flaps produced with this device combination have been previously characterized[15] and were used in the simulations. Preoperative and postoperative maps from Scheimpflug-based tomography (Pentacam; Oculus Optikgeräte GmbH, Wetzlar, Germany) were exported for use in the computational analysis, as described below. The

manufacturer's quality scores for each Pentacam scan were normal and no central data gaps were present. The patient developed postoperative ectasia in his right eye only. He underwent corneal cross-linking in the right eye approximately 20 months after LASIK at a different facility. The left eye remained stable through 3 years of postoperative follow-up.

## Preoperative Finite Element Analysis Simulations

A schematic flowchart of the steps involved in generation of the patient-specific computational models is presented in Figure 1. Tomographic exports and clinical historical data were obtained via retrospective medical chart review, and institutional review board approval was obtained. The research adhered to the tenets of the Declaration of Helsinki.

Preoperative tomography elevation data from the ectatic and unaffected contralateral eyes of the patient were imported into custom finite element meshing software (SpecifEye v0.168; OptoQuest, Cleveland OH). The patient-specific corneal geometry plus a generic limbus and anterior scleral geometry were used to generate each finite element mesh. No difficulties were encountered in interpolating between the available Scheimpflug corneal elevation data and the extracorneal components of the model. Eighth-order Zernike polynomial fits were used to represent the anterior and posterior surfaces of the cornea after mesh generation, and simulated keratometry values were calculated using Vol-CT software (version 7.30; Sarver & Associates, Inc., Carbondale, IL).

To simulate the strain distributions in the preoperative state of the eyes, the discretized geometry including cornea, limbus, and anterior half of the sclera was subjected to an intraocular pressure (IOP) of 15 mm Hg, approximating clinical post-LASIK tonometry values of 14 mm Hg in both eyes at 18 months postoperatively. An iterative procedure[16] was implemented in custom Python code and was used to find the stress-free geometry of the cornea. The model was then subjected to IOP loading to produce the strain distributions of the preoperative state. For simulation of the preoperative state, epithelial and stroma layers were defined separately using different material properties with patient-specific optical coherence tomography-derived total corneal thickness profiles and an assumption of uniform 50-μm epithelial thickness. The epithelium was modeled as hyperelastic incompressible neo-Hookean material using $W = c(I_1 - 3)$, where $I_1$ is the first deviatoric invariant of the left Cauchy-Green deformation tensor and $W$ is the strain energy density function. The value of $c$ was set to 0.002 megapascals (MPa), 5% of the corresponding value for the stroma (see below), to reflect the negligible contribution of the epithelium to the mechanical behavior of the cornea.

The material model used for simulation of the corneal stroma was a microstructurally based fiber-reinforced model proposed by Freed et al.[17,18] with an isotropic neo-Hookean solid matrix. This model takes into account the crimping behavior of collagen fibrils by representing each fiber as a three-dimensional spring. The collagen fibril distribution in the cornea is highly anisotropic and heterogeneous.[19,20] Pinsky et al. proposed an analytical function that captures the main features of the anisotropic collagen fiber distribution.[21] Angular integration of this analytical function was used at each integration point within the model to simulate the gradual change in collagen fiber orientation from the corneal center to its periphery.

The material model equations are summarized here. The strain energy density function in the stroma is defined as:

$$W_{stroma} = W_{matrix} + \frac{1}{\int_{\alpha} \omega(r,\theta,\varphi)} \int_{\alpha} \omega(r,\theta,\varphi) W_{collagen} d\alpha$$

where $r$, θ, and φ define the location and orientation of the fibers in the polar coordinate system within the stroma, α represents the unit sphere, $W$ represents the strain density function, and ω is the fiber distribution function.[21] The stromal matrix is modeled as a neo-Hookean material with the material constant $c$ set to 0.04 MPa.

Cauchy stress of each collagen fiber is given by:

$$\sigma_{collagen} = \frac{1}{I_3^{\lambda}} \frac{\delta W_{collagen}}{\delta \lambda} b(r,\theta,\varphi) \otimes b(r,\theta,\varphi)$$

where $I_3$ is the third deviatoric Cauchy strain invariant, $b$ is fiber orientation vector, and λ is fiber stretch. Freed et al. defined the collagen fiber stress based on a three-dimensional crimped helical fiber assumption, and the equations defining the three-dimensional crimped helical fiber stress can be found in Appendix 1 of that publication.[18] The three parameters of the helical collagen fiber are the initial normalized wavelength of the crimp (set to 30.5), the initial normalized amplitude of the crimp (set to 1.51), and the elastic modulus of the collagen fiber in the linear region, which was set to 32 MPa based on the inverse analysis.

The material model was implemented in an Abaqus UMAT subroutine (Dassault Systems, Johnston, RI). To derive nominal human stromal material constants, the parameters for the model were obtained by performing inverse analyses on previously published human corneal experimental inflation and tensile test data.[23,24] Material properties were iterated using an optimization routine in inflational and tensile simulations until the respective experimental data were replicated. A smooth transition of material properties between cornea, limbus, and sclera was modeled in the study to avoid non-physiologic or abrupt changes in strain distributions. The shear modulus of the cornea was also gradually decreased with increasing depth in accordance with experimental findings[25,26] to more realistically represent the contributions of depth-variant procedures such as LASIK.

## Lasik Finite Element Analysis Simulations

Epithelium, flap, wound, and residual stromal bed layers were each defined in the LASIK models as described previously[26] with case-specific parameters as described in Table 1. The wound layer was modeled as a 10-μm zone at the posterior flap interface and along the lateral circumferential edge of the flap to account for post-healing stromal modifications.[27] The wound assumed complete severing of the collagen fibers for both wound components and a 90% reduction in the shear modulus of the stromal matrix[26] at the deep interface and a 50% reduction in shear modulus for the lateral circumferential edge. A wavefront-optimized ablation formula and transition zone were each implemented for each simulation according to the clinically programmed spherocylindrical refractive treatment. Strain distributions were

obtained using the previously described iterative method. In addition to actual preoperative and simulated postoperative simulations, additional simulations were performed at IOP loading equivalents of 10 and 20 mm Hg to assess differential responses to increased IOP by analyzing the tangential curvature. Interocular differences in the distribution and magnitude of maximum principal strain were assessed, a structural risk variable that characterizes the maximum amount of tensile strain at that material point. Maximum shear strain and von Mises stress were also mapped and compared for each eye.

## Results

Preoperative clinical data are presented in Table 1. Placido-based topography demonstrated mild asymmetric bowtie patterns (Figure A, available in the online version of this article) that were similar for both eyes and incorporated into the ERSS assessment. ERSS scores, percent tissue altered, and surgical parameters including maximum ablation depth, residual stromal bed, and flap thickness are also reported in Table 1. Preoperative and postoperative tomography maps are shown in Figure 2. The fidelity of the preoperative model was confirmed by comparison of clinical and finite element-derived preoperative simulated keratometry values (Table A, available in the online version of this article). Maximum principal strain and maximum shear strain values (dimensionless) at the anterior and posterior surfaces of the residual stromal bed were extracted from the finite element analysis and compared (Figure 3). Strain values were higher in the ectatic right eye in both the preoperative and postoperative states compared to the non-ectatic left eye, with highly asymmetric distributions. Similar patterns were seen in the preoperative and postoperative von Mises stress values (Figure 4). Comparison of actual postoperative simulated keratometry values (37.52/38.40 diopters @ 084) and simulated post-LASIK simulated keratometry values for the unaffected eye (37.70/38.43 diopters @ 081) showed close agreement.

In provocative IOP elevation simulations, the affected eye showed a region of maximal tangential curvature at an IOP of 20 mm Hg in the preoperative state that coincided with the location of ectasia development (Figure 5). The affected eye also showed an IOP-dependent increase in maximum tangential curvature in the preoperative state, whereas the eye that did not develop postoperative ectasia, which was actually steeper at baseline than the eye that eventually developed ectasia, showed a reduction in curvature (Figure 5).

## Discussion

In this study, we present the first clinical application of structural simulation for the analysis of a case of ectasia after LASIK. This computational method combines a geometrically subject-specific model of the cornea derived from clinical tomography, physiologic intraocular loading forces, a fiber-reinforced material formulation that accounts for the three-dimensional spatial orientation of corneal collagen and case-specific LASIK treatment parameters that are applied to the preoperative model to simulate the response to surgery. By offering a comprehensive structural solution of corneal geometry and deformation behavior both before and after LASIK, this approach provided some initial insight into case-specific structural factors in the development of post-LASIK ectasia while illustrating a risk analysis

paradigm that implicitly considers the entire corneal three-dimensional geometry and all its derivatives.

Multiple clinical risk screening paradigms in this case were applied preoperatively or retrospectively and failed to indicate a significant absolute risk of ectasia and/or asymmetry of risk. Comparisons of the contra-lateral eyes using anterior and posterior elevation data and pachymetric distribution did not reveal an absolute risk of ectasia in either eye based on previously established indicators. For example, the Belin-Ambrósio Enhanced Ectasia Display,[13,14] a software feature available on the Pentacam, calculates the Belin-Ambrósio Deviation score (BAD score or D value). The D value was higher for the preoperative LASIK eye that eventually developed ectasia than it was for the contralateral eye. However, the highest D value for either eye was only 1.03 (Table 1), well below the stated threshold for clinical predisposition to ectasia. Similarly, both eyes demonstrated threshold-level values for ectasia risk by the percent tissue altered metric, but with only 5% difference in the values.

Simulations of both eyes in their pre-LASIK states revealed greater preoperative strain and stress magnitudes and more irregular distributions of those variables in the eye that went on to develop ectasia. Both eyes of the modeled patient had similar preoperative geometries and refractive corrections that made preoperative risk assessment more clinically ambiguous and allowed for a meaningful comparison of asymmetry in preoperative and postoperative structural outcomes. Another finding of the post-LASIK simulations was an increase in strain after surgery and a shift in the location of maximum strain from the posterior cornea to the surface of the residual stromal bed. This suggests that after LASIK, the anterior portion of the residual stroma is subjected to additional mechanical loading/deformation and may be more prone to failure if the load exceeds some currently unknown (and probably patient-specific) threshold. Stromal stress was also asymmetrically elevated in the preoperative and postoperative geometries of the eye that developed ectasia, and provides empirical support for the notion that stress may be a correlate of corneal structural risk.[26,28,29]

Strain is an important factor in the tensional homeostasis that drives cellular responses, extracellular matrix maintenance, and remodeling in human connective tissues. Changes in matrix strain have been shown in serum-cultured corneal stromal keratocytes to activate mechanobiological pathways that alter tension in the matrix,[31] and recent cyclic stretching experiments with corneal fibroblasts have shown that strain magnitude determines the balance of expression of matrix metalloproteinases and tissue inhibitors of matrix metalloproteinases such that tissue degradation is favored with higher strains.[37] It is in this sense that we believe strain is a potentially important predictor of the degradative pathways that promote ectasia.

The simulations also predicted directionally opposite changes in corneal curvature as a function of IOP elevation in the fellow eyes. The area of greatest load-dependent steepening in the preoperative simulation of the eye that developed ectasia emerged near the region where postoperative steepening ultimately manifested clinically. In contrast, the preoperative model of the eye that did not develop post-LASIK ectasia demonstrated mild flattening in response to IOP elevation (consistent with prior studies on IOP dependence in normal

eyes[33–35]). These observations provide early proof of concept for differentiation of case-specific risk and represent an important step toward establishing ranges for normal and abnormal/high-risk strains and stresses in larger, population-based finite element studies. It is important to note that these simulations do not include time-dependent material behaviors that are likely to be drivers of the longitudinal changes observed in postoperative ectasia cases.[36] Rather, the results reflect differences in instantaneous load-dependent deformation behaviors that we speculate may be useful in predicting subsequent material failure, which may be mediated by a variety of time-dependent biological and biomechanical responses that have yet to be fully elucidated.[37]

The approach to case-specific LASIK simulation in this study assumed treatment-specific ablation profiles and incorporated optical coherence tomography-derived flap thickness values that were obtained with the same microkeratome by the same surgeon.[16] A parametric analysis exploring the sensitivity of the model predictions to model assumptions was outside the scope of a two-eye report but is planned for a larger cohort with a wider range of patient-specific tomographic inputs to inform the analysis. For the current study, we addressed the issue of model accuracy in the comparison of the post-LASIK simulation results to the actual keratometric outcome for the non-ectatic case. The simulations produced results that closely matched the keratometry values and astigmatic axis for the left eye (Table 2). We were unable to validate the postoperative simulation keratometry values against the actual postoperative data for the affected eye due to unavailability of immediate postoperative scans. The earliest scan available postoperatively for the affected eye demonstrated ectasia at a late stage of progression. To further mitigate the impact of any discrepancies between actual and assumed values for surgical parameters such as ablation profile and flap dimensions, we analyzed risk separately for the preoperative and postoperative states, where the former is not subject to errors associated with surgical assumptions. Both approaches demonstrated asymmetric biomechanical risk favoring ectasia in the affected eye, and this approach allows for separate consideration of intrinsic and extrinsic risk of ectasia.

An obvious limitation of this study is that only one case of unilateral post-LASIK ectasia after bilateral LASIK with preoperative and postoperative tomography was available for modeling. However, the investigative value of this particular clinical case is high given the clinical comparability of the eyes and the failure of some well-established screening paradigms to predict the asymmetric risk of ectasia in the right eye. Another limitation of this study is the absence of patient-specific material properties in the simulations. Although there are ongoing efforts to measure the mechanical properties of the cornea in vivo,[38] techniques capable of obtaining explicit elastic modulus values are not yet clinically available. It is possible that the cornea that developed keratectasia had underlying material property abnormalities that contributed to the unilateral development of ectasia. Due to the absence of patient-specific corneal mechanical properties for these eyes, we assumed that mechanical properties were identical for each eye. The rationale for doing so was to avoid biasing the simulations by assigning arbitrary interocular property differences and to better isolate the predictive performance of three-dimensional structural analysis using only a readily available clinical input. Patient-specific material property data could be included in such simulations when available and would likely add to their predictive value.

Through a high-fidelity finite element modeling approach using clinical tomography data, we were able to observe differences in strain distributions both pre-operatively and postoperatively that were predictive of ectasia development even without explicitly accounting for patient-specific material properties. This analysis represents an important first step toward simulation-based risk assessment and leverages a rare resource: unilateral ectasia cases in which both preoperative and postoperative tomography is available. These simulations reveal intrinsic structural factors that may predispose an eye to complications and can be performed to assess risk in an a priori fashion. Large-scale computational analyses of ectasia risk factors informed by this pilot study are under way.

## Supplementary Material

Refer to Web version on PubMed Central for supplementary material.

## Acknowledgments

Supported in part by NIH grant R01 EY023381 (WJD), an Ohio Third Frontier Innovation Platform Award TECH 13-059 (WJD), an unrestricted grant from Research to Prevent Blindness to the Department of Ophthalmology of the Cleveland Clinic Lerner College of Medicine of Case Western Reserve University, and an unrestricted grant from Research to Prevent Blindness to the University of Southern California Roski Eye Institute Department of Ophthalmology.

## References

1. Randleman JB, Russell B, Ward MA, Thompson KP, Stulting RD. Risk factors and prognosis for corneal ectasia after LASIK. Ophthalmololgy. 2003; 110:267–275.
2. Binder PS, Lindstrom RL, Stulting RD, et al. Keratoconus and corneal ectasia after LASIK. J Cataract Refract Surg. 2005; 31:2035–2038. [PubMed: 16412891]
5. Santhiago MR, Smadja D, Gomes BF, et al. Association between the percent tissue altered and post-laser in situ keratomileusis ectasia in eyes with normal preoperative topography. Am J Ophthalmol. 2014; 158:87–95. [PubMed: 24727263]
6. Santhiago MR, Smadja D, Wilson SE, Krueger RR, Monteiro ML, Randleman JB. Role of percent tissue altered on ectasia after LASIK in eyes with suspicious topography. J Refract Surg. 2015; 31:258–265. [PubMed: 25884581]
7. Santhiago MR, Wilson SE, Hallahan KM, et al. Changes in custom biomechanical variables after femtosecond laser in situ keratomileusis and photorefractive keratectomy for myopia. J Cataract Refract Surg. 2014; 40:918–928. [PubMed: 24726160]
8. Dupps WJ Jr. Ectasia risk: a multifactorial conundrum. J Cataract Refract Surg. 2015; 41:699–700. [PubMed: 25840291]
9. Randleman JB, Woodward M, Lynn MJ, Stulting RD. Risk assessment for ectasia after corneal refractive surgery. Ophthalmology. 2008; 115:37–50. [PubMed: 17624434]
10. Dupps WJ Jr. Ectasia risk: barriers to understanding. J Cataract Refract Surg. 2012; 38:735–736. [PubMed: 22520300]
11. Roberts CJ, Dupps WJ Jr. Biomechanics of corneal ectasia and biomechanical treatments. J Cataract Refract Surg. 2014; 40:991–998. [PubMed: 24774009]
12. Santhiago MR, Smadja D, Gomes BF, et al. Association between the percent tissue altered and post-laser in situ keratomileusis ectasia in eyes with normal preoperative topography. Am J Ophthalmol. 2014; 158:87–95. [PubMed: 24727263]
13. Ambrósio R Jr, Caiado AL, Guerra FP, et al. Novel pachymetric parameters based on corneal tomography for diagnosing keratoconus. J Refract Surg. 2011; 27:753–758. [PubMed: 21800785]
14. Belin MW, Ambrósio R Jr. Corneal ectasia risk score: statistical validity and clinical relevance. J Refract Surg. 2010; 26:238–240. [PubMed: 20415320]

15. Rocha KM, Randleman JB, Stulting RD. Analysis of microkeratome thin flap architecture using Fourier-domain optical coherence tomography. J Refract Surg. 2011; 27:759–763. [PubMed: 21853960]
16. Pandolfi A, Holzapfel GA. Three-dimensional modeling and computational analysis of the human cornea considering distributed collagen fibril orientations. J Biomech Eng. 2008; 130:061006. [PubMed: 19045535]
17. Freed A, Doehring T. Elastic model for crimped collagen fibrils. J Biomech Eng. 2005; 127:587–593. [PubMed: 16121528]
18. Freed AD, Einstein DR, Vesely I. Invariant formulation for dispersed transverse isotropy in aortic heart valves: an efficient means for modeling fiber splay. Biomech Model Mechanobiol. 2005; 4:100–117. [PubMed: 16133588]
19. Boote C, Hayes S, Abahussin M, Meek KM. Mapping collagen organization in the human cornea: left and right eyes are structurally distinct. Invest Ophthalmol Vis Sci. 2006; 47:901–908. [PubMed: 16505022]
20. Meek KM, Quantock AJ. The use of X-ray scattering techniques to determine corneal ultrastructure. Prog Retin Eye Res. 2001; 20:95–137. [PubMed: 11070369]
21. Pinsky PM, van der Heide D, Chernyak D. Computational modeling of mechanical anisotropy in the cornea and sclera. J Cataract Refract Surg. 2005; 31:136–145. [PubMed: 15721706]
22. Elsheikh A, Wang D, Brown M, Rama P, Campanelli M, Pye D. Assessment of corneal biomechanical properties and their variation with age. Curr Eye Res. 2007; 32:11–19. [PubMed: 17364730]
23. Wollensak G, Spoerl E, Seiler T. Stress-strain measurements of human and porcine corneas after riboflavin-ultraviolet-A-induced cross-linking. J Cataract Refract Surg. 2003; 29:1780–1785. [PubMed: 14522301]
24. Petsche SJ, Chernyak D, Martiz J, Levenston ME, Pinsky PM. Depth-dependent transverse shear properties of the human corneal stroma. Invest Ophthalmol Vis Sci. 2012; 53:873–880. [PubMed: 22205608]
25. Sloan SR Jr, Khalifa YM, Buckley MR. The location- and depth-dependent mechanical response of the human cornea under shear loading. Invest Ophthalmol Vis Sci. 2014; 55:7919–7924. [PubMed: 25358729]
26. Sinha Roy A, Dupps WJ Jr, Roberts CJ. Comparison of biomechanical effects of small-incision lenticule extraction and laser in situ keratomileusis: finite-element analysis. J Cataract Refract Surg. 2014; 40:971–980. [PubMed: 24857440]
27. Schmack I, Dawson DG, McCarey BE, Waring GO 3rd, Gross-niklaus HE, Edelhauser HF. Cohesive tensile strength of human LASIK wounds with histologic, ultrastructural, and clinical correlations. J Refract Surg. 2005; 21:433–445. [PubMed: 16209440]
28. Sinha Roy A, Dupps WJ Jr. Effects of altered corneal stiffness on native and postoperative LASIK corneal biomechanical behavior: a whole-eye finite element analysis. J Refract Surg. 2009; 25:875–887. [PubMed: 19835328]
29. Sánchez P, Moutsouris K, Pandolfi A. Biomechanical and optical behavior of human corneas before and after photorefractive keratectomy. J Cataract Refract Surg. 2014; 40:905–917. [PubMed: 24857438]
30. Simonini I, Pandolfi A. Customized finite element modelling of the human cornea. PloS One. 2015; 10:e0130426. [PubMed: 26098104]
31. Petroll WM, Miron-Mendoza M. Mechanical interactions and crosstalk between corneal keratocytes and the extracellular matrix. Exp Eye Res. 2015; 133:49–57. [PubMed: 25819454]
32. Liu C, Feng P, Li X, Song J, Chen W. Expression of MMP-2, MT1-MMP, and TIMP-2 by cultured rabbit corneal fibroblasts under mechanical stretch. Exp Biol Med (Maywood). 2014; 239:907–912. [PubMed: 24939826]
33. Dupps WJ Jr, Roberts C. Effect of acute biomechanical changes on corneal curvature after photokeratectomy. J Refract Surg. 2001; 17:658–669. [PubMed: 11758984]
34. Pierscionek BK, Asejczyk-Widlicka M, Schachar RA. The effect of changing intraocular pressure on the corneal and scleral curvatures in the fresh porcine eye. Br J Ophthalmol. 2007; 91:801–803. [PubMed: 17151057]

35. Villas-Bôas FS, Doi LM, Sousa AK, Melo LA Jr. Correlation between diurnal variation of intraocular pressure, ocular pulse amplitude and corneal structural properties. Arq Bras Oftalmol. 2009; 72:296–301. [PubMed: 19668956]

36. Dupps WJ Jr. Biomechanical modeling of corneal ectasia. J Refract Surg. 2005; 21:186–190. [PubMed: 15796225]

37. Dawson DG, Randleman JB, Grossniklaus HE, et al. Corneal ectasia after excimer laser keratorefractive surgery: histopathology, ultrastructure, and pathophysiology. Ophthalmology. 2008; 115:2181–2191. [PubMed: 18692245]

38. Scarcelli G, Besner S, Pineda R, Kalout P, Yun SH. In vivo biemechanical mapping of normal and keratoconus corneas. JAMA Ophthalmol. 2015; 133:480–482. [PubMed: 25611213]

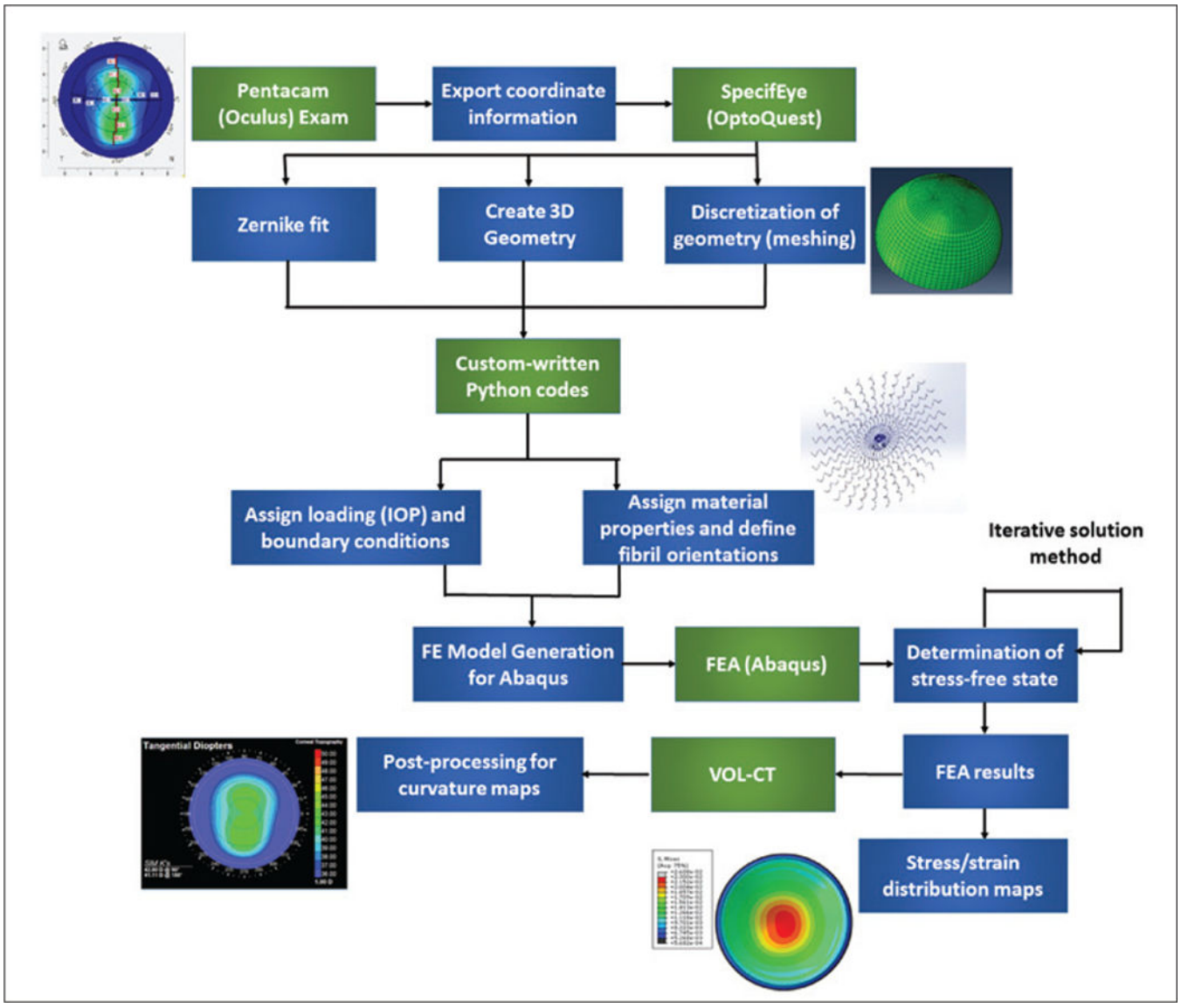


**Figure 1.**

Schematic flowchart of the steps used in patient-specific computational modeling of corneal refractive surgery ectasia cases. IOP = intraocular pressure; FE = finite element; FEA = finite element analysis; VOL-CT = VOL-CT software (Sarver & Associates, Inc., Carbondale, IL)

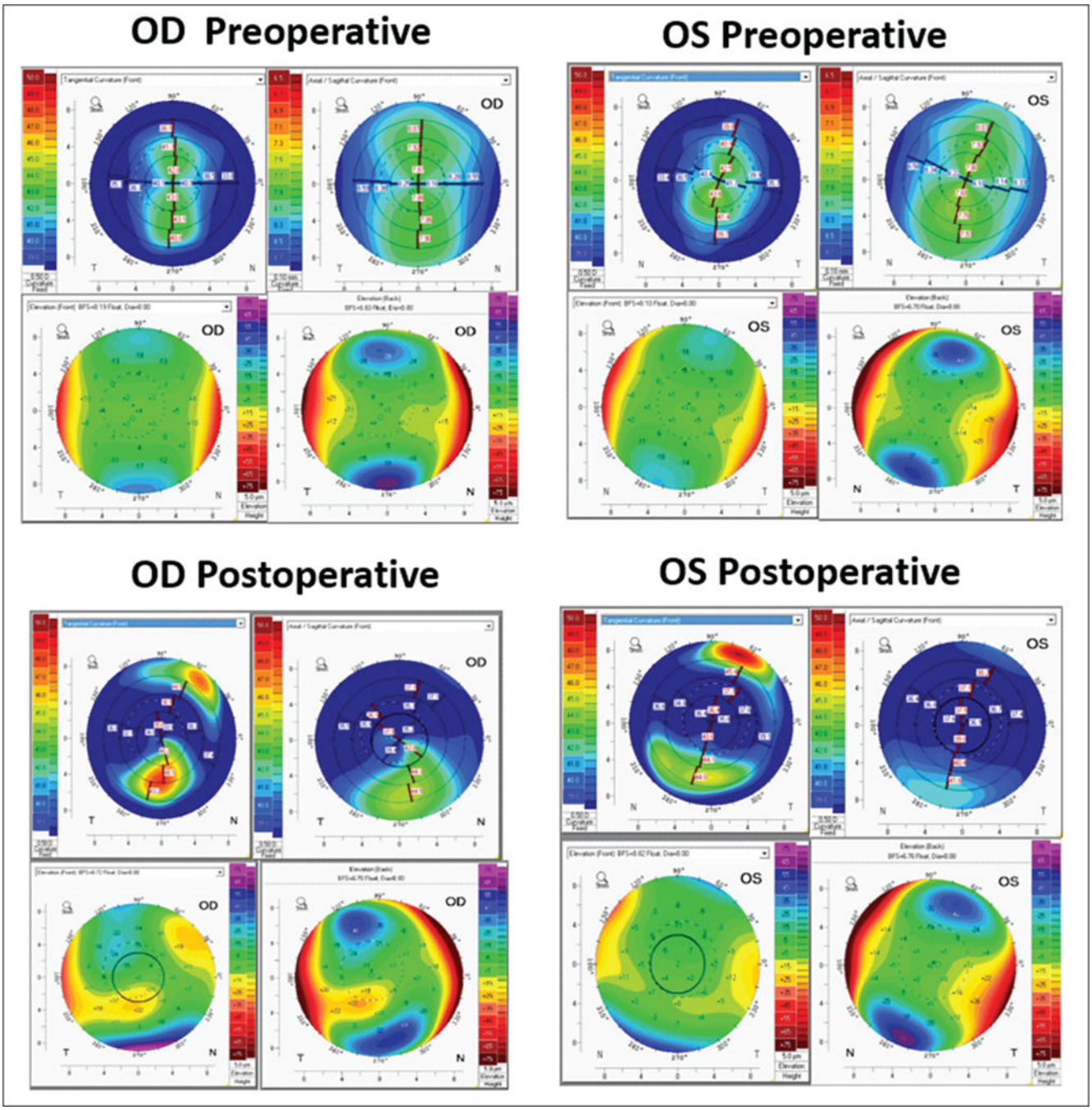


**Figure 2.**

Preoperative and postoperative tomography maps from the Pentacam HR (Oculus Optikgeräte GmbH, Wetzlar, Germany) showing anterior tangential curvature, axial curvature, back and front elevation (clockwise order from top left). Preoperative differences were minimal between the (A) right (OD) and (B) left (OS) eye. Postoperatively, differential inferior steepening is seen in the (C) ectatic right eye in comparison to the (D) stable left eye.

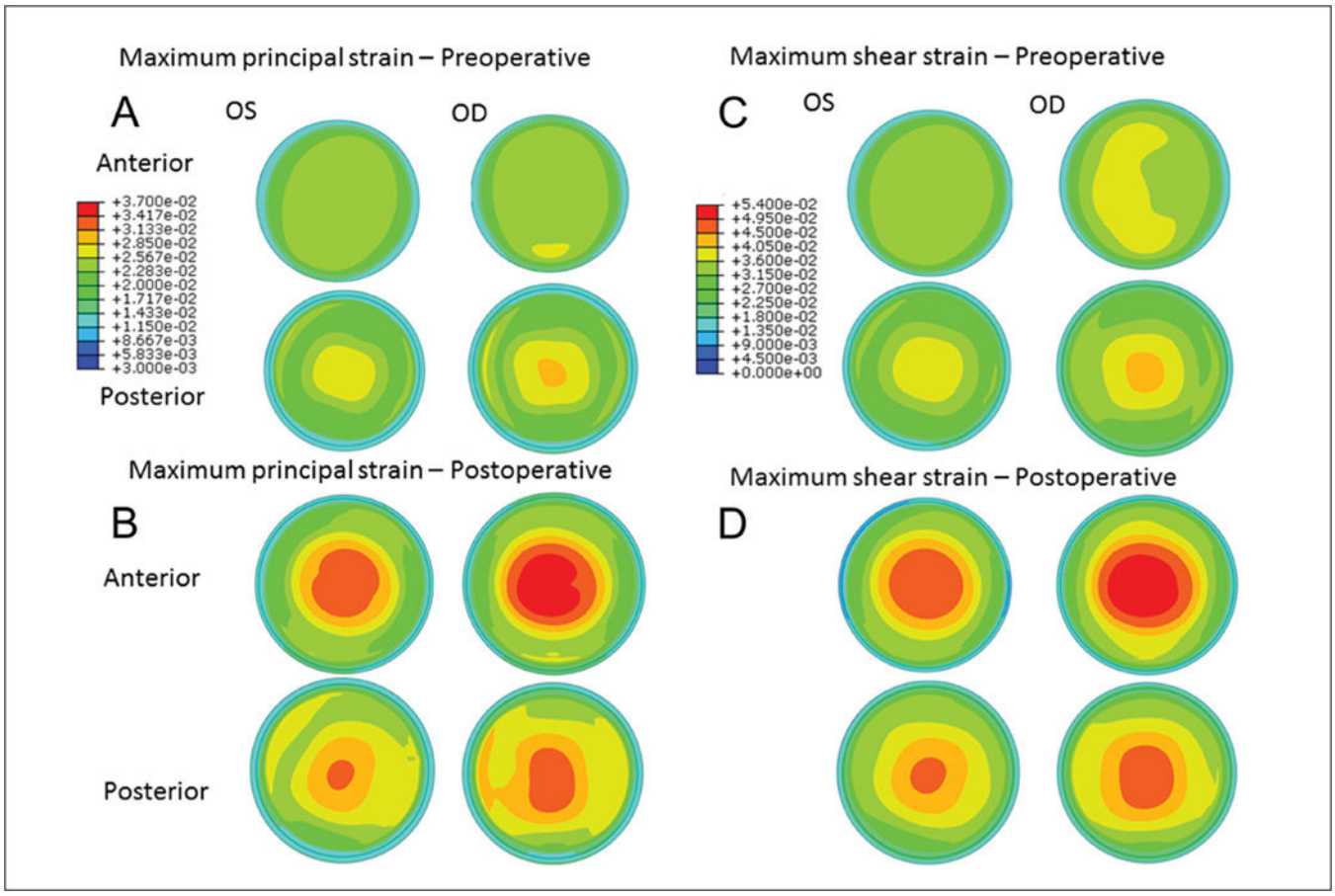


**Figure 3.**

Maps of maximum principal strain from the anterior and posterior stromal surfaces in the (A) preoperative and (B) simulated postoperative state. Higher strain values, larger areas of increased strain, and more eccentric distributions of strain are apparent in all states and in all regions in the eye that ultimately developed ectasia (right eye [OD]). An inferior region of locally concentrated strain was predicted in the postoperative state of the OD where the ectatic region manifested clinically (A). Highest focal maximum principal strain values (dimensionless units) from the anterior residual stromal bed were 0.038 in the left eye (OS) and 0.042 in the OD in the preoperative state, and 0.049 and 0.053, respectively, in the postoperative state. Maximum shear strain was also highly asymmetric in (C) preoperative and (D) postoperative models between eyes throughout the stroma and favored greater shear strain in the eye that eventually developed ectasia.

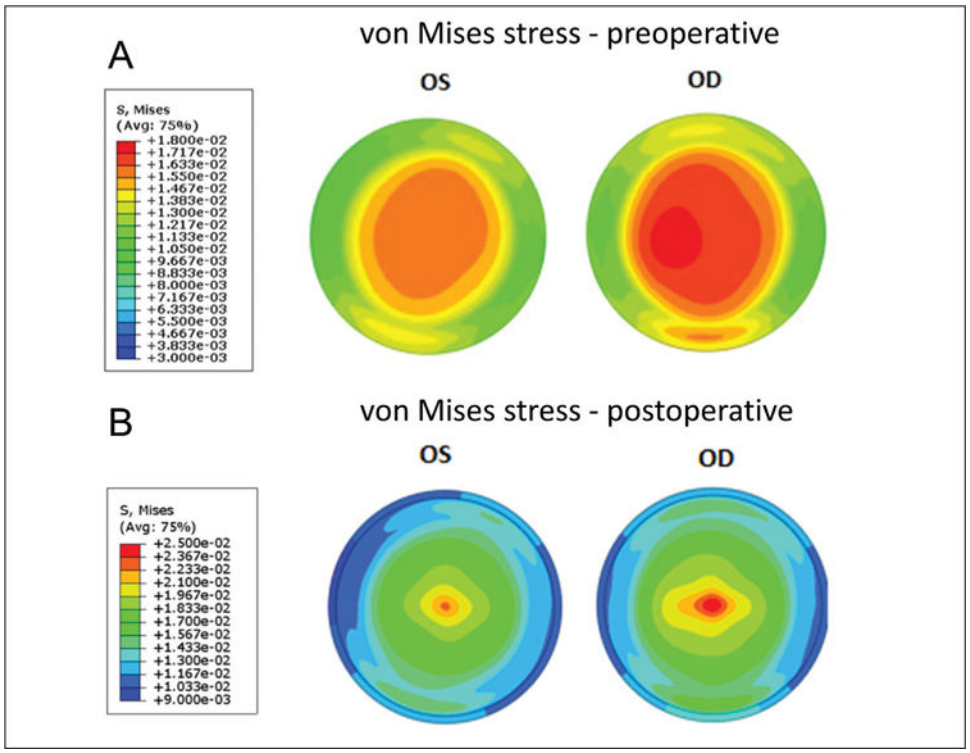


**Figure 4.**

Maps of von Mises stress (in megapascals, MPa) from the anterior stroma in the (A) preoperative state and the (B) anterior residual stroma in the simulated post-LASIK state. Higher stress magnitudes as well as larger and more eccentric areas of peak stress are present before and after simulated LASIK in the eye that ultimately developed ectasia (right eye [OD]). Color scales are different for the preoperative and postoperative states to facilitate visualization of the interocular differences. OS = left eye

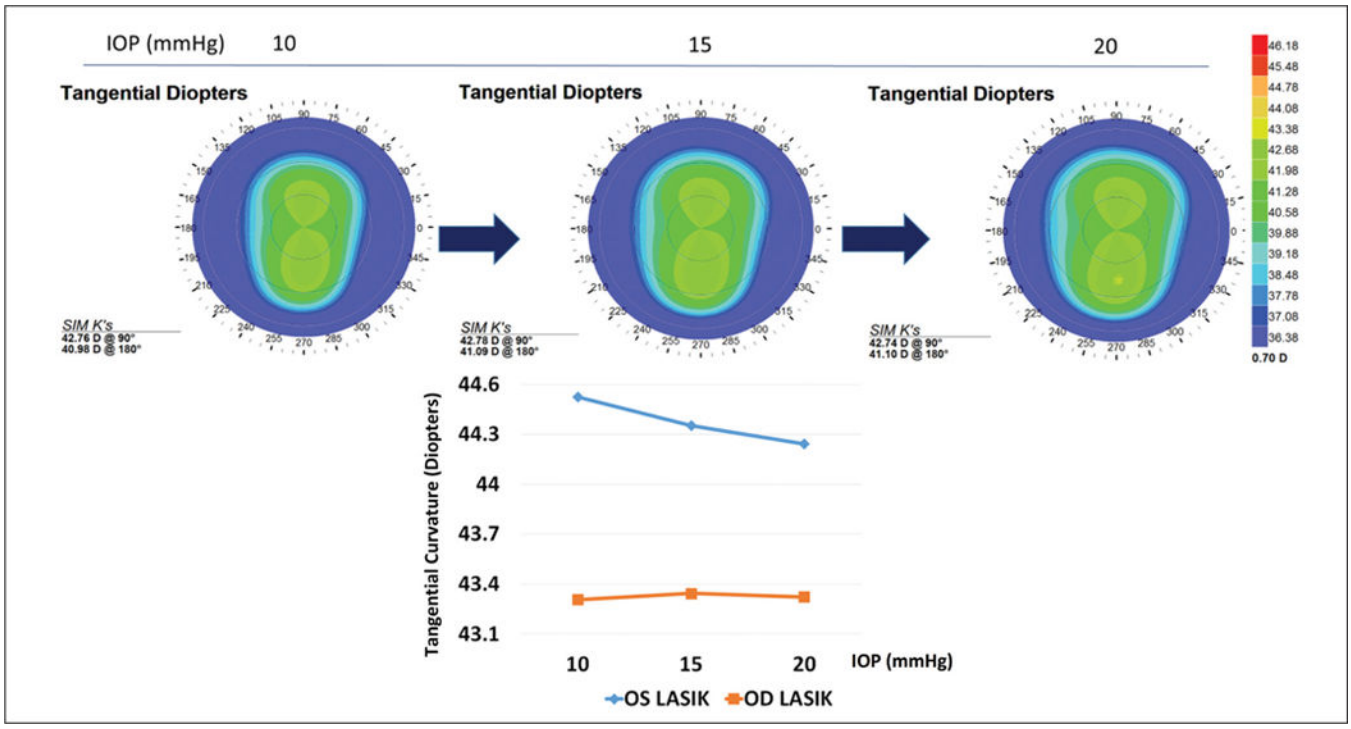


**Figure 5.**

Change in tangential curvature due to increasing intraocular pressure (IOP) in the preoperative state of the eye that ultimately developed ectasia (upper row). Maximum tangential dioptric power as a function of simulated IOP elevation in the preoperative models of both eyes (lower row). The eye that ultimately developed ectasia (OD) demonstrated a nonlinear increase in the curvature of the steepest point, in contrast to the reduction in dioptric (D) power observed in the contralateral eye over the same pressure interval. OD = right eye; OS = left eye; SIM K = simulated keratometry values

**Table 1**

Preoperative Patient and Procedure Data, ERSS Variables, and PTA Values

| Variable | Right Eye (Ectasia) | Left Eye (No Ectasia) |
|---|---|---|
| ERSS age category | ≥ 30 years (0) | ≥ 30 years (0) |
| Axial topography pattern (score) | Asymmetric bowtie (1) | Asymmetric bowtie (1) |
| Preoperative MRx (score) | −6.75 +2.00 × 084 (0) | −6.25 +2.00 × 065 (0) |
| CCT (μm) (score) | 495 (2) | 508 (2) |
| RSB thickness (μm) (score) | 290 (1) | 299 (1) |
| Total ERSS | 4 | 4 |
| PTA | 42 | 40 |
| Maximum ablation depth (μm) | 98 | 92 |
| Flap thickness (μm) | 110 | 110 |
| Belin-Ambrósio D score[a] | 1.03 | 0.55 |
| IOP (mm Hg) | 13 | 15 |

ERSS= Ectasia Risk Score System; PTA = percent tissue altered; MRx = manifest refraction; CCT = central corneal thickness; RSB = residual stromal bed; IOP = intraocular pressure

[a]Both values for D score were subthreshold for indicating risk according to the device user instructions.

**Table 2**

Comparison of Preoperative Clinical Curvature Data and Finite Element Analysis-Generated Curvature Data for Model Verification

| **Preoperative clinical data Simulated K (Diopters)** | | **Preoperative model Simulated K (Diopters)** |
|---|---|---|
| OS | 41.40/43.60@ 69 | 41.35/43.60 @ 69 |
| OD | 41.10/42.80@ 90 | 41.09/42.78 @ 90 |